


RESEARCH

Open Access

# Effect of genomic and cellular environments on gene expression noise



Clarice K. Y. Hong<sup>1,2†</sup>, Avinash Ramu<sup>1,2†</sup>, Siqi Zhao<sup>1,2†</sup> and Barak A. Cohen<sup>1,2\*</sup> 

<sup>†</sup>Clarice KY Hong, Avinash Ramu, and Siqi Zhao contributed equally to the manuscript.

\*Correspondence: [cohen@wustl.edu](mailto:cohen@wustl.edu)

<sup>1</sup>The Edison Family Center for Genome Sciences and Systems Biology, School of Medicine, Washington University in St. Louis, Saint Louis, MO 63110, USA

<sup>2</sup>Department of Genetics, School of Medicine, Washington University in St. Louis, Saint Louis, MO 63110, USA

## Abstract

**Background:** Individual cells from isogenic populations often display large cell-to-cell differences in gene expression. This “noise” in expression derives from several sources, including the genomic and cellular environment in which a gene resides. Large-scale maps of genomic environments have revealed the effects of epigenetic modifications and transcription factor occupancy on mean expression levels, but leveraging such maps to explain expression noise will require new methods to assay how expression noise changes at locations across the genome.

**Results:** To address this gap, we present Single-cell Analysis of Reporter Gene Expression Noise and Transcriptome (SARGENT), a method that simultaneously measures the noisiness of reporter genes integrated throughout the genome and the global mRNA profiles of individual reporter-gene-containing cells. Using SARGENT, we perform the first comprehensive genome-wide survey of how genomic locations impact gene expression noise. We find that the mean and noise of expression correlate with different histone modifications. We quantify the intrinsic and extrinsic components of reporter gene noise and, using the associated mRNA profiles, assign the extrinsic component to differences between the CD24+ “stem-like” substate and the more “differentiated” substate. SARGENT also reveals the effects of transgene integrations on endogenous gene expression, which will help guide the search for “safe-harbor” loci.

**Conclusions:** Taken together, we show that SARGENT is a powerful tool to measure both the mean and noise of gene expression at locations across the genome and that the data generated by SARGENT reveals important insights into the regulation of gene expression noise genome-wide.

## Background

Gene expression is noisy, even among individual cells from an isogenic population [1]. Noisy gene expression leads to variable cellular outcomes in differentiation [2–5], the response to environmental stimuli [6, 7], viral latency [8], and chemotherapeutic drug resistance [9–11]. Explaining the causes of noisy expression remains an important challenge.



© The Author(s) 2024. **Open Access** This article is licensed under a Creative Commons Attribution 4.0 International License, which permits use, sharing, adaptation, distribution and reproduction in any medium or format, as long as you give appropriate credit to the original author(s) and the source, provide a link to the Creative Commons licence, and indicate if changes were made. The images or other third party material in this article are included in the article's Creative Commons licence, unless indicated otherwise in a credit line to the material. If material is not included in the article's Creative Commons licence and your intended use is not permitted by statutory regulation or exceeds the permitted use, you will need to obtain permission directly from the copyright holder. To view a copy of this licence, visit <http://creativecommons.org/licenses/by/4.0/>. The Creative Commons Public Domain Dedication waiver (<http://creativecommons.org/publicdomain/zero/1.0/>) applies to the data made available in this article, unless otherwise stated in a credit line to the data.

A gene's genomic environment, defined here as the composition of nearby *cis*-regulatory elements and local epigenetic marks, can influence its expression noise. Some features of genomic environments that can affect noise include enhancers, histone modifications, and transcription factor (TF) occupancy [12–18]. These observations raise the possibility that genome-wide patterns of expression noise could be explained using the large-scale epigenetic maps that have proved useful in explaining mean expression levels [19–21]. Leveraging these resources to explain expression noise will require maps of the genome that show the influence of diverse genomic environments on this noise. Producing these maps will require new experimental approaches because the existing studies demonstrating the effects of epigenetic marks on expression noise have either been performed on endogenous genes, where the effects of different chromosomal locations are confounded with the effects of the different endogenous promoters, or rely on low-throughput imaging methods. Dar et al. assayed the noisiness of large numbers of genomic integrations, but was unable to assign genomic locations to the measured reporter genes [15]. Two other studies have assayed integrations in a high-throughput manner but measured protein levels by flow cytometry rather than mRNA levels [22, 23]. Even for the same reporter gene, noise in translational mechanisms can confound the measurements [24], especially when trying to understand the impact of features that regulate transcription. Thus, we still lack a high-throughput, systematic way of quantifying the impact of genomic environments on expression noise.

In addition to intrinsic features such as the local genomic environment, extrinsic features, such as the global cellular state of a cell, can also influence gene expression noise [25–29]. For example, variation in the cell cycle, cell size, or signaling pathways can all impact gene expression noise [1, 30, 31]. However, the relative contributions of intrinsic vs extrinsic features on gene expression noise in mammalian cells remains unclear.

Here we report Single-cell Analysis of Reporter Gene Expression Noise and Transcriptome (SARGENT), a highly parallel method to measure the mean and noise of a common reporter gene that has been integrated at locations across the genome. Analysis of SARGENT data showed that different histone modifications explain the mean and noise produced across the genome. In SARGENT, multiple reporters are integrated in each cell, allowing us to separate the intrinsic and extrinsic contributions to noise. A key advantage of SARGENT is that we can also sequence the associated single-cell mRNA transcriptomes, further enabling us to attribute the extrinsic noise to differences in the cellular substates between isogenic cells. To our knowledge, this is the largest genome-wide survey of the impact of intrinsic and extrinsic noise in gene expression. Taken together, our results show that SARGENT is a powerful tool to study how genomic environments and cellular context control expression noise.

## Results

### A high-throughput method to measure mean and noise across the genome

We developed a high-throughput method to test the effects of genomic environments on the mean and noise of gene expression. Our goal was to integrate a common transgene across the genome and then, for individual cells, measure both the transcripts produced from the transgene and the global mRNA profile. This allows us to compute the mean and noise of reporter gene expression at each location and correlate reporter gene

expression with the cellular mRNA state of each cell. Because every unique integration contains the same transgene, the measured differences in the mean and noise of reporter gene expression are directly attributable to the influence of genomic environments or cellular states.

We first generated a reporter gene with a library of 16 bp random barcodes (location barcode, locBC) in its 3'UTR (Fig. 1). Due to the diversity of the locBCs, each locBC is only associated with a single location in the genome [20]. The reporter gene consists of a cytomegalovirus (CMV) promoter driving the expression of a fluorescent protein and contains a capture sequence from the 10× Genomics Single Cell Gene Expression 3' v3.1 with Feature Barcoding Kit. We chose to use the CMV promoter because it is a general promoter that should respond to different enhancers and chromatin environments. The 10× gel beads contain both the complementary capture sequence and polyT sequences, allowing us to isolate the transcripts produced from the reporter gene and the cellular transcriptome.

To generate chromosomal integrations across the genome, we cloned the reporter gene library onto a piggyBac transposon vector. We selected the piggyBac transposon system

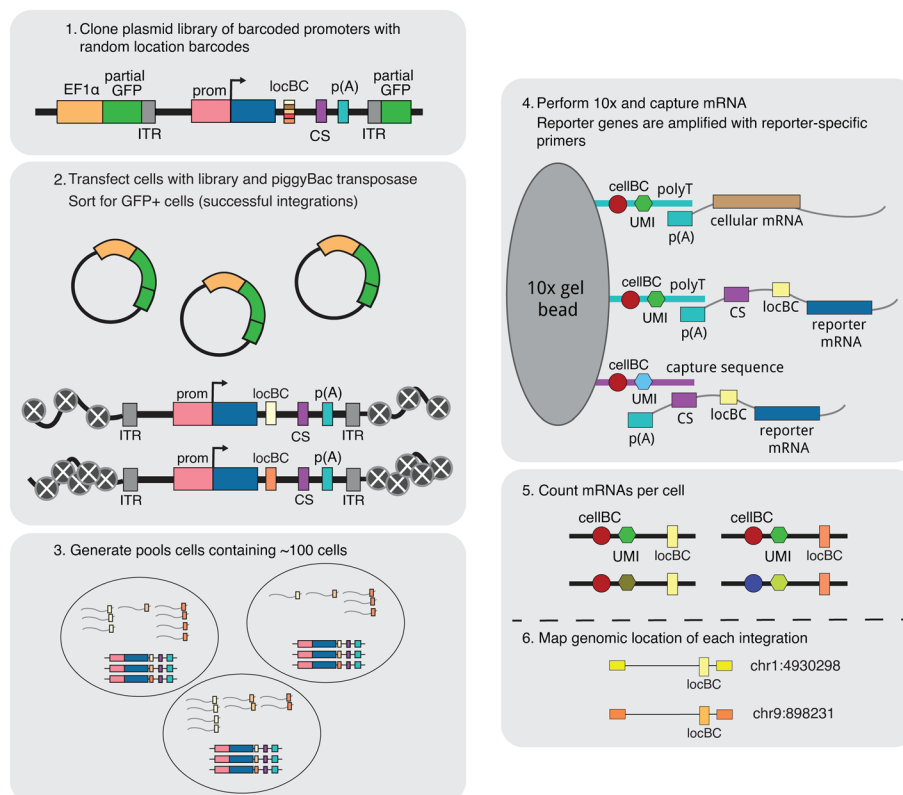


**Fig. 1** Overview of the SARGENT workflow. In step 1, a reporter gene driven by the CMV promoter is randomly barcoded with a diverse library of location barcodes (locBC) upstream of the 10× capture sequence (CS). The reporter genes are randomly integrated into K562 cells and sorted for cells with successful integrations (step 2), then sorted again after a week into pools to ensure that each barcode is only represented once per pool (step 3). We then performed scRNA-seq to capture the transcriptome and amplify the expressed barcodes from integrated reporter genes (step 4). The number of expressed barcodes per cell were then tabulated (step 5). To identify the genomic locations of the integrations, we also mapped the location of each locBC with inverse PCR (step 6). ITR: inverted terminal repeat, prom: promoter

because it has a bias towards active chromatin regions where transcription is more likely to occur so that we are likely to detect the IRs by scRNA-seq. The library was transfected into cells along with piggyBac transposase to allow random integrations of the reporter into the genome. We performed SARGENT in K562 cells because of the abundance of public epigenetic data available for this cell line. After sorting the transfected cells for integrations, we mapped the locations of each integrated reporter (IR) and assigned each locBC to a specific genomic location. We then captured the reporter gene transcripts from single cells and amplified the barcodes (10× cell barcode, UMI, and locBC) using primers specific to our reporter gene (Fig. 1, “Methods”). After sequencing and tabulating the mRNA counts for each IR, we computed the expression level of the reporter gene at each genomic location in each single cell. For a subset of cells, we also sequenced the mRNA profiles to simultaneously reveal the cell state of each individual cell.

#### **SARGENT measurements are accurate and reproducible**

We first assessed the reproducibility of the SARGENT method. Because replicate infections result in pools of cells with insertions at different genomic locations, we could not assess the reproducibility of independently transfected pools of cells. Instead, we assessed the reproducibility of SARGENT by growing the same pool of insertions (Pool 4) in separate flasks and performing the SARGENT workflow independently on each sample. We detected 589 identical IR locations in both replicates, which represented 96% of the total IRs observed in both replicates. After quality control, we obtained data from 7680 single cells across replicates, and a total of 2,940,912 unique molecular identifiers (UMIs) representing expressed barcodes from the IRs in these cells. The replicates were well correlated for measurements of both mean and noise measured at each IR location (Fig. 2A, B, mean Pearson’s  $r = 0.76$ , noise Pearson’s  $r = 0.72$ ) indicating that measurements obtained by SARGENT are reproducible. We combined the two technical replicates from Pool 4 for downstream analysis.

To validate the single-cell measurements made by SARGENT, we also performed single-molecule fluorescence in situ hybridization (smFISH) on two known locations. At least for these two locations, the measurements of mean and variance made by smFISH qualitatively agree with the SARGENT measurements for those locations (Additional file 1: Fig. S1) suggesting that our method is accurate and reproducible for measuring the mean and noise of expression.

#### **Measurements of mean-independent noise across different chromosomal environments**

In total, we performed four experiments and generated mean and noise measurements for 939 integrations (Additional file 2: Table S1). The integrations were spread across the genome and found in regions with different chromHMM annotations [32] (Additional file 1: Fig. S2A, S2B), allowing us to study the effects of diverse chromosomal environments on expression noise. The mean and variance of expression are often highly correlated [33, 34]. Similarly, we found a strong correlation between the mean and variance in SARGENT data, indicating that a large proportion of an IR’s noise is explained by its mean level of expression (Fig. 2C). To identify chromosomal features that control expression noise independent of mean levels we regressed out the effect of mean levels on noise, leaving us with a metric we refer to as mean-independent noise (MIN) [33]. By

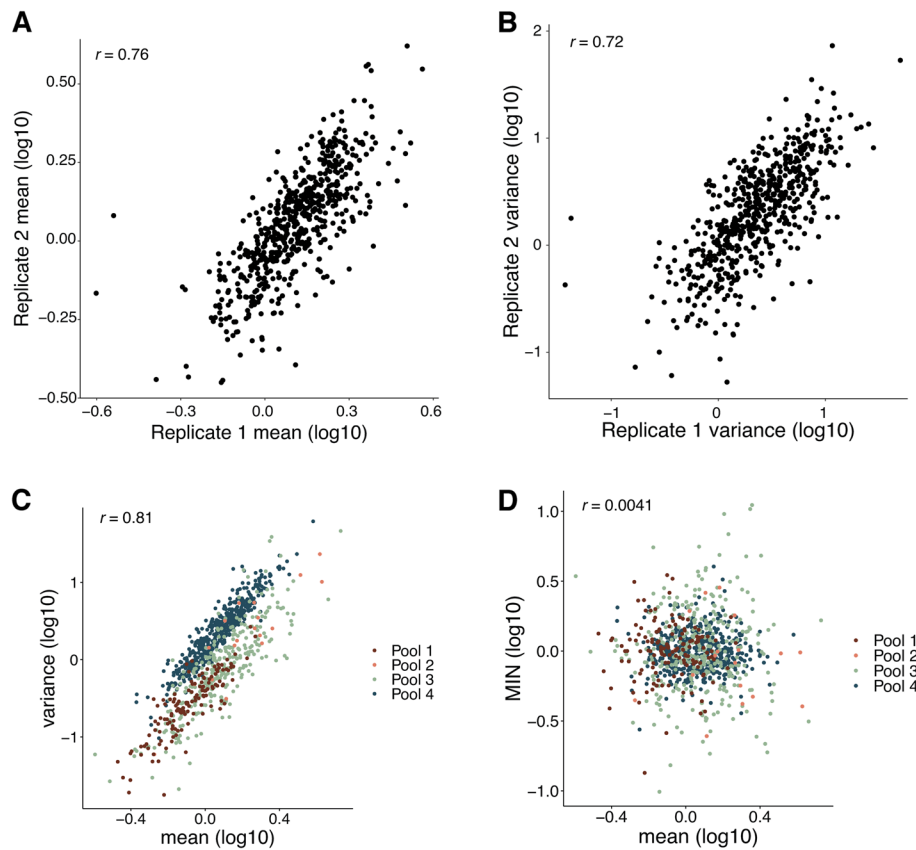


**Fig. 2** SARGENT measurements are accurate and reproducible. **A** Correlation of mean levels between technical replicates. **B** Correlation of variance measurements between replicates. **C** Mean and variance are correlated within each experiment. **D** Mean-independent noise corrects for mean effects on variance. Correlations shown are Pearson's correlation coefficients (Pearson's  $r$ )

design, MIN levels of IRs are uncorrelated with their mean expression levels (Fig. 2D) whereas other measures of noise, such as the coefficient of variation or the Fano factor, retain residual correlation with mean levels in our data (Additional file 1: Fig. S2C, S2D). Thus, we used MIN as a measure of expression noise for all following analyses.

### Expression mean and noise are associated with different chromosomal features

We sought to identify chromatin features that would explain differences in MIN levels between genomic locations. Studies of genome-wide chromatin features in many cell lines and tissues have shown that the mean expression of a gene is correlated with its surrounding chromatin marks [20, 35]. Thus, we asked whether chromatin features might also explain patterns of MIN across the genome. We split the IRs into bins of high or low mean levels, or high or low MIN levels, and identified chromatin features that were correlated with each bin. As expected, IRs with high mean expression had higher levels of active chromatin marks such as H3K27ac, H3K4 methylation, H3K79me2, and H3K9ac (Fig. 3A). Conversely, IRs with high MIN did not exhibit differences between H3K27ac or H3K4me1 levels, and low MIN locations showed slightly elevated levels of H3K4me2/3, H3K79me2, and H3K9ac (Fig. 3B). To ensure that these results are not due to the presence of outlier IR locations, we also plotted the mean levels of each chromatin

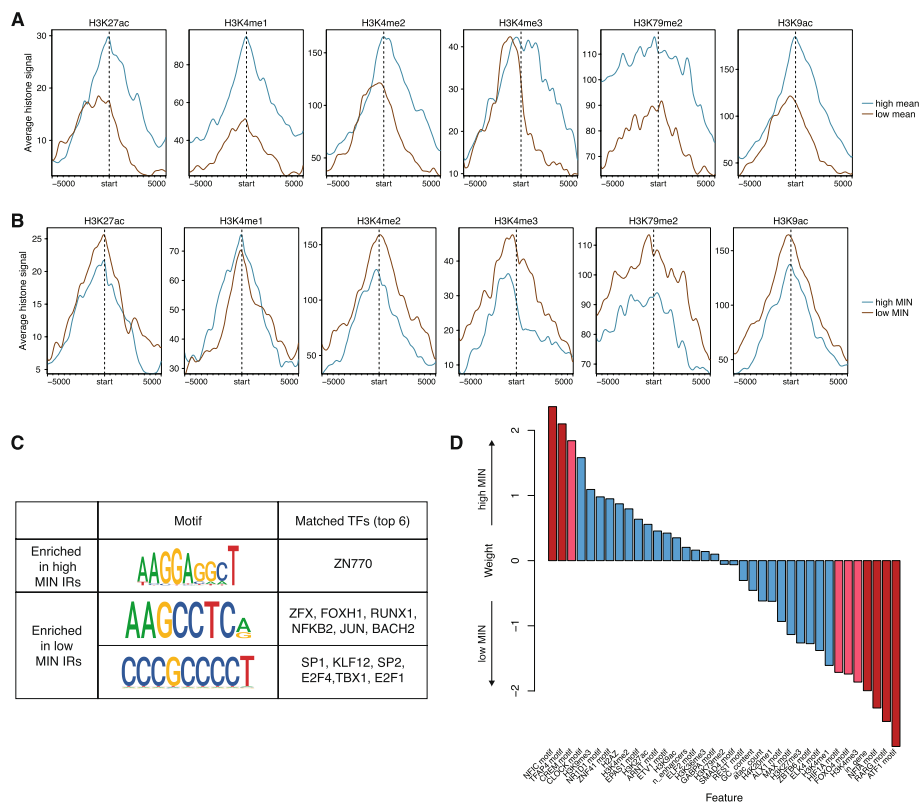


**Fig. 3** Expression mean and noise are associated with different chromosomal features. **A** Active histone modifications associated with high or low mean IRs. Start indicates the location of the IR, and each location was extended 5 kb on either side. IRs that map to the minus strand were reverse complemented so the orientation with respect to the IR is consistent. **B** Active histone modifications associated with high or low MIN IRs are different from those associated with mean. **C** Motifs enriched in high or low MIN IRs respectively (STREME [36]  $p$ -value < 0.05), and potential TFs that match these discovered motifs. **D** Logistic regression weights of various intrinsic features associated with high or low MIN IRs. Red bars:  $p$ -value < 0.05; pink bars:  $0.05 < p$ -value < 0.1 from the logistic regression model

mark for each IR and showed that there are no individual IR locations that appear to be skewing the distribution (Additional file 1: Fig. S3A, S3B). We also randomly permuted the mean/MIN labels to determine the significance of the differences we observed. For high/low mean levels, the differences observed for all chromatin modifications are significant, while for MIN levels, only H3K4me2/3 and H3K9ac are significant (Additional file 1: Fig. S3C), suggesting that the differences observed above are robust. These results suggest that different chromatin modifications influence the mean and noisiness of expression and that more active genomic locations might also reduce MIN. This observation is consistent with previous studies showing that repressed chromatin is associated with high MIN [18, 22].

The binding of TFs also impacts noise in gene expression. To identify TFs that might affect noise, we identified motifs whose occupancy is enriched near either high or low MIN IRs. Sequences at low MIN IRs are enriched for motifs that are bound by transcriptional activators such as SP1 and E2F4, while sequences at high MIN IRs are enriched for motifs that are bound by other TFs including TFs containing basic helix-loop-helix

(bHLH) domains (Fig. 3C), suggesting that the cofactors recruited by different TFs have separable effects on expression mean and noise. To further understand whether the identified motifs are functioning across multiple regions or are only enriched in a few regions, we plotted the distribution of occurrences of each motif in each region. Depending on the motif, each motif can occur ~0–5 times. Motifs enriched in high MIN regions occur in more high MIN regions and at slightly higher frequency in high MIN regions, while low MIN motifs are present in more low MIN regions (Additional file 1: Fig. S3D, 3E). These results suggest that the TFs binding to these motifs act across many high/low MIN regions to modulate gene expression noise.

To assess the power of genomic features to predict the MIN of IR locations, we trained a logistic regression model using various chromatin modifications, sequence features, and genomic annotations to classify high and low MIN locations (total 37 features, full list of features in Additional file 3: Table S2). The model achieved 59% accuracy using leave-one-out cross-validation (LOOCV). The features with significant weights are the H3K4me3 mark, TF motifs (RARG, FOXO4, HIF1A, TFAP4, CREM, ATF1, NFIC, and NFIA), and whether the IR location was inside a gene (Fig. 3D, Additional file 3: Table S2). Being inside a gene reduced the probability of being a high noise IR location, which could be due to local regulatory elements that might dampen gene expression noise for robust expression. Similar to our results above, lower H3K4me3 increased the probability of being a high noise IR location. H3K4me3 is associated with active chromatin and supports the hypothesis that higher activity reduces IR MIN. Our observation is consistent with a previous study showing that H3K4me3 correlates with reduced noise at endogenous genes [18]. With respect to the effects of TFs on noise, the presence of some TF motifs increases the probability of being a high noise IR location (NFIC, CREM, TFAP4, CLOCK), whereas other TFs reduce the probability of being a high noise location (RARG, NFIA, ATF1, FOXO4, HIF1A).

We used a similar logistic regression framework to identify features that separate IR locations with high or low mean levels of expression. The model accuracy is 66% using LOOCV. The chromatin features that increase the probability of being a high mean IR location are lower levels of H3K27me3, lower levels of H3K4me2, and a higher number of ATAC-seq peaks, which agrees with the known effects of these features in bulk mean expression. The motifs that increased the probability of being a high mean IR location are higher numbers of motifs of the ZNF76, BACH1, and E2F3 TFs and fewer instances of the E2F7, SMAD3, and SOX5 motifs. (Additional file 1: Fig. S3F, Additional file 4: Table S3). Comparisons of the models explaining either mean or noise again show that different genomic features are correlated with gene expression mean and noise.

#### **Intrinsic and extrinsic factors have similar effects on gene expression noise**

Expression noise caused by fluctuations in global factors affects all genes and is referred to as extrinsic noise, whereas intrinsic sources of noise are specific to individual genes [22, 28–31, 33]. The correlation between identical reporter genes in the same cell measures the balance between extrinsic and intrinsic noise, with extrinsic factors increasing the correlation [25]. In SARGENT, the correlation between IRs in the same cells is a measure of extrinsic factors that affect noise across IR locations.

For our analysis of extrinsic noise, we first identified IRs in the same clonal cells using the co-occurrence of locBCs between single cells. We identified 192 clones, with a mean of three integrations per clone (Additional file 1: Fig. S4A, Additional file 5: Table S4). Of these 192 clones, 45 contain more than one integration (Fig. 4B), making them suitable for an analysis of extrinsic noise. To validate the identified clones, we individually mapped IR barcodes in 16 clones and found that 94% of the individually mapped IR locations could be uniquely assigned to an identified clone (Fig. 4B).

We next asked if extrinsic factors also contribute to the observed gene expression noise. For each cell in a clone, we calculated the coefficient of variation (CV) which is the standard deviation relative to the mean of all IRs in that cell. Lower fluctuation indices indicate that the IRs in a clone fluctuate in sync (high extrinsic noise), while higher CVs indicate that each IR varies independently (high intrinsic noise). To simulate intrinsic noise, we first shuffled the cell labels of all the IRs within a clone and computed a distribution of CVs for the shuffled population. If all the measured noise was intrinsic, then the measured distribution would perfectly overlap the shuffled distribution. If all the measured noise was extrinsic, then all the cells would have CVs of 0 (Additional file 1: Fig. S4B). We found that all clones show a distribution of CVs that is lower than that of the shuffled distribution and above zero (Additional file 1: Fig. S4C). This suggests that some portion of the expression noise can be explained by extrinsic factors that impact all IRs within a cell in different genomic environments.

To quantify the contribution of intrinsic and extrinsic noise in each clone we employed an established statistical framework [37]. Using the pairwise IR single cell expressions for all clones that contain more than one IR as input, we found that intrinsic noise comprises approximately 54% of the total noise (Fig. 4C, D). This analysis suggests that both the intrinsic chromatin and extrinsic cellular context explains

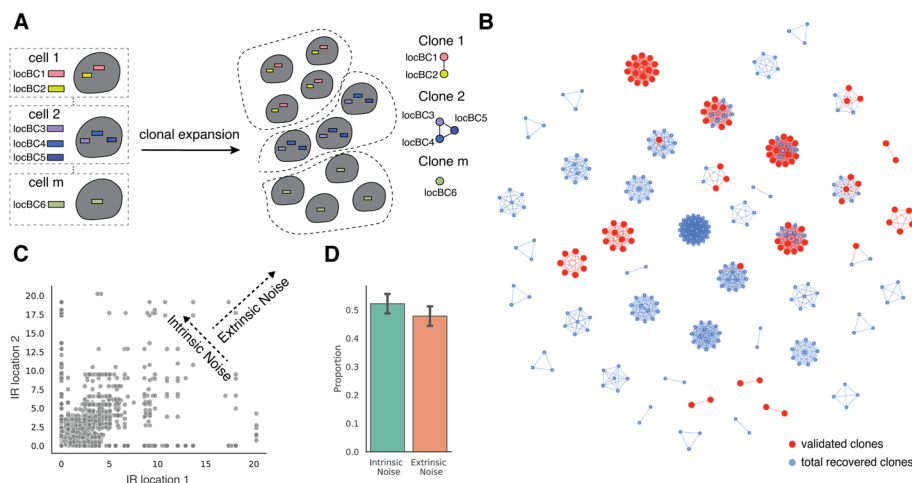


**Fig. 4** SARGENT quantifies the extrinsic portion of expression noise. **A** Schematic for identifying different initial clones. **B** A network representation of the different clones identified; red nodes indicate IR locations that were independently validated by sequencing individual clones. **C** Expression of pairs of IR locations from the same cell. Correlation between pairs of IR locations suggests that they are co-fluctuating and indicate the presence of extrinsic noise, while the anti-correlation suggests that the IRs are fluctuating independently and indicate the presence of intrinsic noise. **D** Quantification of intrinsic and extrinsic proportion of noise. Error bars from two technical replicates



about half of the total noise in each clone. These results show that SARGENT can quantify both intrinsic and extrinsic contributions to expression noise.

### Cell substates are a source of expression noise

What cellular mechanisms control expression noise? We hypothesized that differences between cellular substates within isogenic populations are an important source of noise. Isogenic K562 cells transition between “stem-like” and “more differentiated” substates [38, 39]. The stem-like substate is marked by high CD24 expression and proliferates at a higher rate, which we hypothesized would contribute to extrinsic noise. This hypothesis predicts that the same IRs will have higher MIN in stem-like cells compared to more differentiated cells. To test this prediction, we sequenced the single-cell transcriptomes associated with 356 of the 939 genomic locations in parallel with the IRs. Using the transcriptomes, we identified clusters of cells with high CD24 expression and confirmed that these clusters had the signatures of high-proliferating cells (Additional file 1: Fig. S5A, S5B). We then calculated the expression mean and MIN for each IR location separately in the two substates. Contrary to our prediction, IR locations in the stem-like substate have higher mean and lower MIN (Fig. 5A, B). This suggests that the global differences between the two substates are a source of MIN, but this is not due to differences in proliferation rates.

Given the differences in mean and MIN between the substates, the MIN of the IR locations in a given clone should be partly explained by the proportion of its cells in each substate. Consistent with this prediction, we found that clones with a higher proportion of cells in the stem-like substate have slightly higher average mean expression (Spearman's  $\rho = 0.22$ ,  $p$ -value = 0.008), and lower average MIN (Spearman's  $\rho = -0.27$ ,  $p$ -value = 0.0015) across all IRs in the clone (Fig. 5C, D). We hypothesized that this was due to the slightly higher proliferation rates of cells in the stem-like phase. As expected, there are more cells in the S phase in the stem-like substate compared to the more differentiated state (Fig. 5E). We then examined the differences of mean and MIN in different cell cycle phases and found that expression mean is higher and MIN is lower in the S phase compared to other phases (Additional file 1: Fig. S5C, 5D). These results suggest that differences in proliferation rates is an important source of extrinsic noise, and that SARGENT is a powerful tool to dissect the extrinsic sources of expression noise.

### Cellular information improves classification of low vs high MIN IR locations

Since extrinsic factors play an important role in determining expression noise, we trained a logistic regression model to predict MIN using three extrinsic features (proportion of cells in S, proportion of cells in G2, and proportion of CD24<sup>+</sup> cells). Using only the global features, the model achieved 75% accuracy using LOOCV. This result implies that these cellular features explain a significant portion of the variance in MIN between high and low IR locations. The proportion of cells in G2 and the proportion of cells in the CD24<sup>+</sup> state were significant predictors in this model (Additional file 3: Table S2). Being in G2 increases the probability of a high MIN IR location [40] whereas having a higher proportion of CD24 cells reduces the probability of being a high MIN IR location (Fig. 5F). When we combined the significant intrinsic features from the previous model with these extrinsic features, the model accuracy dropped slightly to 73%

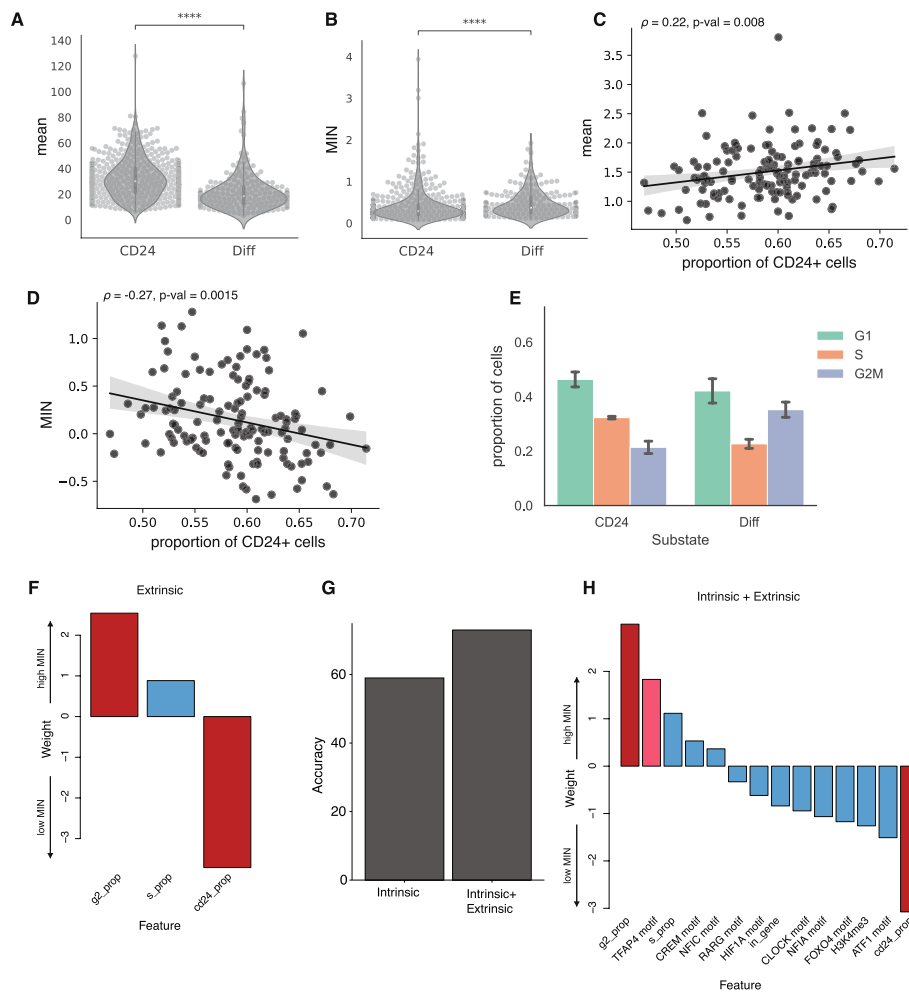


**Fig. 5** Cellular information improves classification of low vs high MIN IR locations. **A, B** Violin plots of expression mean and MIN at two substates (Student *t*-test, \*\*\*\* $p < 0.0001$ ), each dot is an IR location. **C, D** Scatterplots of proportion of cells in the “stem-like” substate against mean and MIN; each dot is the average mean expression or MIN from a clone. Line: linear fit with 95% CI. Spearman correlation between mean and proportion of cells in the “stem-like” substate: 0.22,  $p$ -value = 0.008. Spearman correlation between MIN and proportion of cells in the “stem-like” substate:  $-0.27$ ,  $p$ -value = 0.0015. **E** Barplot of the fraction of cells in different cell cycle phases for cells in the “stem-like” substate and the “differentiated” substate (Binomial test: S phase  $p < 2.2e-16$ , G1 phase  $p < 5.9e-5$ , G2M phase  $p < 2.2e-16$ ). The error bars are derived from the two replicates. **F** Weights of logistic regression model using extrinsic (cellular) features alone. **G** Addition of extrinsic features helps to improve the accuracy of the model. **H** Weights of logistic regression model using both intrinsic and extrinsic features. The most significant features are still the proportion of cells in the G2 phase and CD24<sup>+</sup> phase. Red bars:  $p$ -value  $< 0.05$ ; pink bars:  $0.05 < p$ -value  $< 0.1$  from the logistic regression model

(using LOOCV) suggesting that the extrinsic features are sufficient to capture the effects of the intrinsic features on MIN (Fig. 5G). In the combined model, the extrinsic features have higher weights than the intrinsic genomic environment features (Fig. 5H), suggesting that the cell-state information may play a larger role in regulating MIN compared to genomic environments.

We observed a similar role for extrinsic features in classifying IR locations with high mean levels from IR locations with low mean levels. Using LOOCV, the model accuracy

for just the extrinsic feature model is 76% and increases to 80% for the combined model with both intrinsic and extrinsic features (Additional file 1: Fig. S5E). In the combined model, the proportion of cells in the CD24 cell-state is the most highly weighted feature (Additional file 1: Fig. S5F, Additional file 4: Table S3). In contrast to the MIN model, the proportion of cells in the CD24 state increases the probability of being a high-mean IR location (Fig. 5H, Additional file 1: Fig. S5F), which is consistent with our observations in Fig. 5B and D. Thus, while cellular information plays an important role in gene expression regulation, these features have orthogonal impacts on expression mean and single-cell variability.

### Effects of transgenes integration on endogenous genes

Finally, SARGENT can be used for purposes beyond studying gene expression noise. One such application is screening for “safe harbor” loci in the genome. To achieve safe and effective gene therapy, we need to identify genomic locations that have stable expression of the transgene of interest (high mean expression and low noise) and have minimal effects on endogenous gene expression. Historically, transgenes are often integrated into several known “safe harbor” loci [41]. Those loci are mainly located in the introns of stably expressed genes to prevent silencing. Because SARGENT can be used to measure gene expression mean, noise and endogenous gene expression simultaneously, we can leverage SARGENT to screen for potential safe harbors in a high-throughput manner.

We examined how our reporter gene integrations altered the expression of the gene into which it integrated. We focused on the 65 IR locations that are integrated into gene bodies (Additional file 6: Table S5). These integrations were distributed across different clones (Additional file 1: Fig. S6A) and should not be confounded by clonal effects. We calculated pseudo-bulk expression for each gene from clones that contain the integration and compared that to the expression from other clones that do not have the IR integration (Fig. 6A). We found that in most cases (61/65), transgene integration does not alter the endogenous gene expression (Fig. 6B). We also randomly shuffled the gene labels to compute the background differential expression and found that there were no significantly differentially expressed genes once the labels were shuffled (Additional file 1: Fig. S6B). Among the locations with significantly differentially expressed genes, three out of four IR integrations increase gene expression (Fig. 6C), consistent with previous studies showing that the integration of a transgene often increases endogenous gene expression [42]. Taken together, our results suggest that most endogenous genes are not impacted by the integration of exogenous genes. This result illustrates that SARGENT could be a powerful tool to screen for “safe harbor” loci for transgene integration.

### Discussion

Since the early single-cell studies showing the variability of gene expression in isogenic populations [25], many individual chromatin and sequence features have been suggested to modulate expression noise [1, 5, 43, 44]. However, there has yet to be a systematic study of the impact of different genomic features on large numbers of identical genes.

We developed SARGENT, a high throughput method to measure the expression mean and noise at different genomic locations in parallel. One key advantage of SARGENT is that the reporter gene used in all locations is identical, which allows us to isolate the

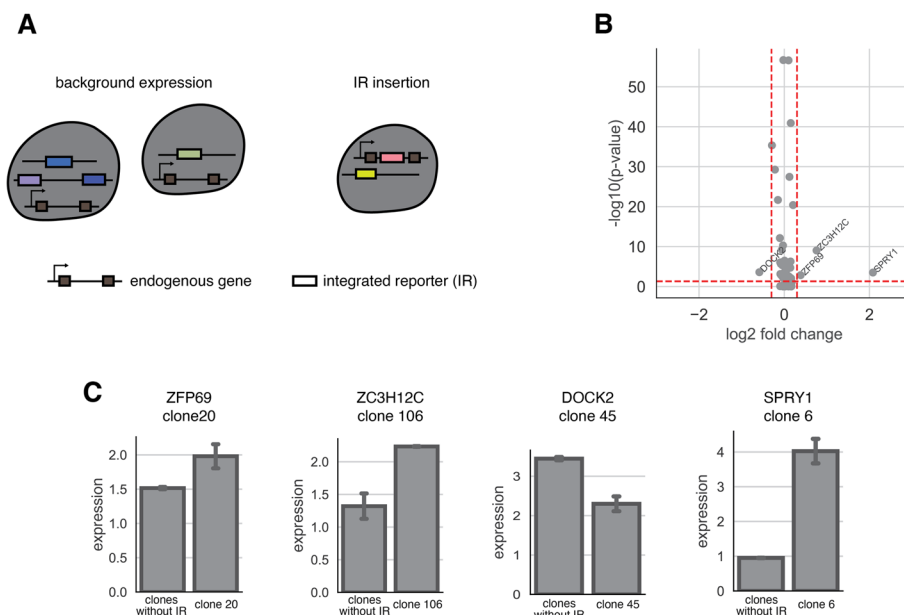


**Fig. 6** SARGENT measures the insertion effect of a transgene. **A** Schematic for expression change detection in the transcriptome data. **B** Volcano plot of log<sub>2</sub> fold change and -log<sub>10</sub>(p-value) from a Fisher’s exact test. Red dotted line: cutoff for fold change (0.5), cutoff for p-value: 0.05. Four genes (labelled) pass both thresholds. **C** Barplots of difference of expression between genes without IRs (control) and genes with IRs (insert). The clone where the IR is integrated is indicated. Error bars are derived from two technical replicates

effects of the genomic environments without being confounded by the effects of different promoters. We measured the expression mean and noise of >900 reporter genes at known locations, which is substantially more than previous studies [23]. We identified different chromatin marks that are associated with high or low MIN and used a logistic regression model to identify features of the genomic environments that might control MIN. Our observations indicate that the features that control expression noise are independent of the features controlling expression mean. Several recent studies have developed tools for the orthogonal control of mean and gene expression noise [43, 45, 46]. To this end, our results suggest potential mechanisms that can be targeted for independent modulation of expression mean and single-cell variability.

We also quantified the extrinsic portion of expression noise and identified that the oscillation between a “stem-like” substate and a “differentiated” substate in K562 cells is an important source of extrinsic noise. Our data suggests that extrinsic noise might be more important in regulating MIN than genomic environments. This indicates that the regulation of noise of individual genes might be at the level of the promoter, rather than through its chromatin or genomic environment.

We envision that SARGENT will be a useful tool for other synthetic biology applications. While advances in genome engineering technologies now allow researchers to integrate transgenes at most desired genomic locations, the selection of appropriate sites for transgene overexpression remains non-trivial, with no location in human cells validated as a safe harbor locus [42, 47]. This is mainly due to the lack of methods to systematically screen for loci that have high expression, low variability, and do not impact cellular function. Here we showed that SARGENT can be used to read out a transgene’s

impact on global expression as well as the endogenous gene that it is integrated into. With SARGENT, we can quickly screen genomic locations to find the best locations for human transgene integration which will prove useful in gene therapy applications.

## Conclusions

We envision that SARGENT will be a useful technology for many different applications including mechanistic studies of gene expression noise and synthetic biology applications. The 10× Genomics platform used in this study is limited by throughput, but improvements to scRNA-seq technologies will increase the scope of SARGENT. For example, coupling sci-RNA-seq [48] or SPLiT-seq [49] to SARGENT would allow for many more locations to be assayed in parallel. A larger goal will be to construct a detailed map of the MIN landscape across the genome.

## Methods

### SARGENT library cloning

All primers and oligonucleotides used in this study are listed in Additional file 7: Table S6. To clone the reporter gene for SARGENT, we first cloned a CMV-BFP reporter gene containing the 10× capture sequence 1 (CS1) into a piggyBac vector containing two parts of a split-GFP reporter gene [50]. When the reporter gene construct is integrated into the genome, the split-GFP combines to produce functional GFP, allowing us to sort for cells that have successful reporter gene integrations. We next added a library of random barcodes to the plasmid by digesting the plasmid with XbaI followed by HiFi assembly (New England Biolabs) with a single-stranded oligo containing 16 random N's (location barcodes; locBC) and homology arms to the plasmid (CAS P57).

### Generation of cell lines for SARGENT

K562 cells were maintained in Iscove's modified Dulbecco's medium (IMDM) + 10% FBS + 1% non-essential amino acids + 1% penicillin/streptomycin. The cell line was obtained from the Genome Engineering and Stem Cell Center at Washington University in St. Louis, which performs cell line authentication by STR testing, and is routinely tested for mycoplasma. We selected two K562 cell lines previously used in our lab that each contain a "landing pad" at a unique location with a pair of asymmetric Lox sites for recombination (loc1 - chr8:144,796,786, loc2 - chr11: 16,237,204; hg38 coordinates). Using these "landing pad" cell lines allows us to perform smFISH on the landing pad to directly compare SARGENT and smFISH results. For each cell line, we replaced the original landing pad cassette with the same reporter gene in the SARGENT library so that we can capture the reporters from the landing pad and reporters from other genomic locations in SARGENT using the same primers. Pool 1 was derived from the loc2 cell line, while Pools 2, 3, and 4 were derived from the loc1 cell line.

The SARGENT library and a plasmid expressing piggyBac transposase (gift from Robi Mitra lab) were co-transfected into K562 (LP cell lines) cells at a 3:1 ratio using the Neon Transfection System (Life Technologies). For each experiment, we transfected 2.4 million cells with 9 µg of SARGENT library and 3 µg of transposase plasmid. If the reporter gene successfully integrates into the genome, the two parts of the GFP reporter on the plasmid recombine produce GFP. The cells were sorted after 24 h for GFP+ cells to

enrich for cells that have integrated SARGENT reporters. We reasoned that ~100 single cells for each Integrated Reporter (IR) location would be required to obtain a good estimate of mean and variance. Each SARGENT experiment contains many single-cell clone expansions: all the cells from the same clone share the same genomic integrations. Since we targeted approximately 20,000 cells per 10× run, the upper limit of the numbers of clones we can test in one experiment is 200. Because 10× also has a high dropout rate, we targeted 100 clones per experiment in order to ensure that we obtained high quality data. Each clone has an average of five integrations, which theoretically allows us to assay 500 IR locations in one experiment. Since the clones did not all grow at the same rate, practically, we obtained fewer than 500 IRs per experiment.

For Pools 1 and 2, cells were sorted into pools of 100 cells each and allowed to grow until there were sufficient cells for RNA/DNA extraction and SARGENT experiments. Pool 3 contained the same cells as Pool 2, except that single cells were allowed to grow individually in 96-well plates and pooled by hand just before the SARGENT experiments. This allowed for a more even representation of each individual clone (which contains unique integrations) in the final pool. For Pool 4, transfected cells were first sorted into 96-well plates with 2 cells/well and allowed to grow individually and 100 wells were manually pooled for SARGENT experiments. We used cells from Pool 4 to compute technical reproducibility.

#### **SARGENT integration mapping**

We harvested DNA from SARGENT pools using the TRIzol reagent (Life Technologies). To map the locations of SARGENT integrations, we digested gDNA for each pool with a combination of AvrII, NheI, SpeI, and XbaI for 16 h. The digestions were purified and self-ligated at 16°C for another 16 h. After purifying the ligations, we performed inverse PCR to amplify the barcodes with the associated genomic DNA region (CAS P59 and P64). For each pool, we performed two technical replicates with eight PCRs per replicate and pooled the PCRs of each replicate for purification. We then used 8 ng of each replicate for further amplification with two rounds of PCR to add Illumina sequencing adapters (CAS P55 and P65). The sequencing library was sequenced on the Illumina NextSeq platform.

The barcodes of each read were matched with the sequence of its integration site. The integration site sequences were then aligned to hg38 using BWA [51] with default parameters. Only barcodes that mapped to a unique location were kept for downstream analyses. All barcodes and IR locations can be found in Additional file 2: Table S1.

#### **ClampFISH**

Single-molecule FISH was performed on the two “landing pad” locations that were in the original cell lines used for SARGENT (see “Generation of cell lines for SARGENT” above). ClampFISH probes for the reporter genes were designed using the Raj Lab Probe Design Tool (rajlab.seas.upenn.edu, Additional file 8: Table S7). Each probe was broken into three arms to be synthesized by IDT. The 5′ of the left arm is labeled by a hexynyl group, and the 3′ of the right arm is labeled by NHS-azide. The right arm fragment was purified by HPLC. All three components were resuspended in nuclease-free H<sub>2</sub>O to a concentration of 400 μM. The three arms were ligated by T7 ligase (NEB, Cat# M0318L)

at 25 °C overnight, then purified using the Monarch PCR and DNA cleanup Kit (NEB, Cat# T1030S), and eluted with 40 µl of nuclease-free water. After the ligation, each probe is stored at −20 °C. ClampFISH was performed according to the suspension cell line protocol of clampFISH [52]. 0.7 million cells were collected and fixed in 2 mL of fixing buffer containing 4% formaldehyde for 10 min, then permeabilized in 70% EtOH at 4 °C for 24 h. The primary ClampFISH probes were then hybridized for 4 h at 37 °C in the hybridization buffer (10% Dextran Sulfate, 10% Formamide, 2× SSC, 0.25% Triton X). After hybridization, cells were spun down gently at 1000 rcf for 2 min. Cells were washed twice with the washing buffer (20% formamide, 2× SSC, 0.25% Triton X) for 30 min at 37 °C. The secondary probes were then hybridized to cells at 37 °C for 2 h and the cells were then washed twice with washing buffer for 30 min at 37 °C. The primary and secondary probes are “clamped” in place through a click reaction (CuSO<sub>4</sub> 75 µM, BTAA 150 µM, Sodium Ascorbate 2.5 mM in 2X SSC) for 20 min at 37 °C. The cells were then washed twice in the washing buffer at 37°C for 30 min each wash. Then, the cells were hybridized with the hybridization buffer with tertiary probes for 2 h at 37°C. We complete 6 cycles of hybridization for all our experiments. After the final washes, cells were incubated at 37 °C with 100mM DAPI for 20 min, washed twice with PBS, resuspended in the anti-fade buffer, and spun onto a #1.5 coverslip (part number) using a cytospin cytocentrifuge (Thermo Scientific), mounted onto a glass slide, sealed with a sealant, and stored at 4°C.

### **SARGENT library using the 10× genomics platform**

#### ***Cell preparation***

We used the Chromium Single Cell 3' Kit (v3.1) from 10× Genomics for SARGENT. We followed the manufacturer's instructions for preparing single-cell suspensions. We used a cell counter to measure the number of cells and viability and used cell preparations with greater than 95% cell viability.

#### ***Cell barcoding and reverse transcription***

We followed the manufacturer's instructions with the following modifications in Pools 1–3: no 10× template switching oligo (PN3000228) was added to the Master Mix (Step 1.1). To correct for the missing volume, 2.4 µl of H<sub>2</sub>O was added to the master mix per reaction. For Pool 4, the template switching oligo was included as written. For the cDNA amplification (Step 2.2), no 10× provided reagents were used. Instead, a custom primer (CAS P20) was used with 14 cycles of amplification with the provided 10× protocol (Step 2.2 d). For the pool where we also sequenced transcriptomes (Pool 4), we followed the 10x protocol as written for cDNA amplification.

#### ***Barcode PCR and library preparation***

We performed nested PCRs to amplify barcodes from 10× cDNA. For Pools 1–2, PCR library construction was split into two pools for amplification of transcripts captured by capture sequence 1 and poly(A), respectively. Both PCR reactions were done with 2 µl purified cDNA, 2.5 µl 10 µM reporter-specific forward primer (CAS P45), 2.5 µl 10 µM poly(A) (CAS P20) or capture sequence adapter-specific primers (CAS P32), and 25 µl Q5 High Fidelity 2× Master Mix (M0492, New England Biolabs) in 50 µl total volume with 10 cycles amplification. The PCRs were then purified with Monarch PCR and

DNA Cleanup Kit (New England Biolabs, T1030) and Illumina adapters were added in another 2 rounds of PCR, with a PCR purification step with the Monarch kit between PCRs. For poly(A) amplicons, we used CAS P42 and CAS PP2, followed by CAS P48 and CAS PP4. For capture sequence amplicons, we used CAS P41 and CAS CS2, followed by CAS P48 and CAS CS4. The reactions were then pooled and purified with SPRIselect Beads (Beckman Coulter) at 0.65× volume. For Pool 4, we performed the PCRs for the poly(A) fraction using 2 µl purified cDNA as described above, but not the capture sequence transcripts.

## **SARGENT data processing**

### ***Read parsing***

We first identified the reads that match the constant sequence in our reporter gene. We used two versions of constant sequence to match against, depending on if the read was captured using the poly(A) sequence on the mRNA or the capture sequence specific to the 10× beads. We used a fuzzy match algorithm `fuzzysearch` (<https://github.com/taleinat/fuzzysearch>) with a Levenshtein distance cutoff of 2 to capture reads that have a mismatch at these positions due to sequencing error. From each read, we parsed out the cell barcode, 10× UMI and locBC by absolute position in the read. The 16-bp-long cell barcode and the 12-bp-long UMI are obtained from the first 28 positions in Read1; the locBC is obtained from the appropriate position after the end of the reporter gene in Read2. We then collapsed reads with identical cell barcodes, UMI and locBCs into one “trio” and kept track of the number of reads supporting each trio. For downstream analysis, we filtered out trios with only one supporting read since these are likely to be enriched for PCR artifacts (mean trio read depth across all pools is 9.5). We next processed the trios to error correct the cell barcodes and locBCs before estimating the mean and variance.

### ***Barcode error correction***

To correct for PCR artifact and sequencing errors, a custom script was used to error-correct for 10× cell barcodes. Briefly, we first acquired the empirical distribution of the Hamming distances among observed 10× cell barcodes. We found that more than 99% of 10× cell barcode pairs have a Hamming distance greater than 6, making error correction a feasible approach to denoise the data. We first identify cell barcodes that match perfectly to the 10× cell barcode whitelist, then we order them based on their abundance of number of reads. The cell barcodes that are not in the whitelist are then compared to the ordered whitelisted cell barcodes, if the Hamming distance between the non-whitelisted cell barcodes is within 2 Hamming distances of a whitelisted cell barcodes, we correct the non-whitelisted cell barcode. With cell barcode correction, we recovered ~12% of reads that would have been discarded.

Due to the random synthesis of the locBC, a slightly different approach was taken for error correction for the locBCs. Briefly, all the locBCs are ranked based on abundance of number of reads. Starting from the most abundant barcode, we look for locBCs that are within 4 Hamming distance to that barcode and correct them. We then remove



that barcode and any corrected barcodes and repeat this process until we have iterated through all locBCs.

#### ***Calculating mean and variance of each IR***

For cells from Pool 4 with single-cell transcriptome data, we used CellRanger 6.0.1 to identify a list of valid cell-barcodes before applying the additional filtering steps listed here. For cells from the other pools without single-cell transcriptome data, the filters were directly applied. We filtered out cells that had less than five IR integrations (locBCs) and less than ten UMIs in order to remove cell barcodes that are not associated with intact cells captured in the droplets similar to the standard 10× single-cell transcriptome analysis. We also filtered out locBCs that were seen in less than five cells and UMIs that had less than two supporting reads. Using these filters, we are potentially removing some lowly expressed locations that are expressed in very few cells. However, this ensures that the locations we retain and use for downstream modeling are better powered to measure mean and variance. These filters were chosen to maximize reproducibility between replicates. We then computed the number of UMIs per locBC in each cell to calculate the expression level of each locBC. We normalize the UMI count by the total number of UMIs per cell to adjust for variable capture efficiency between cells—cells with more UMIs per cell have higher capture efficiency and hence better chance of detecting a UMI. We also normalize by the UMI counts by total number of locBCs in a cell—cells with more locBCs have a slightly lower chance of being detected in our assay so we correct for this.

Normalization factor for cell  $j$  = Total number of UMIs detected in cell  $j$  / Total number of locations in cell  $j$

Normalized UMI count for location  $i$  in cell  $j$  = Number of UMIs for location  $i$  in cell  $j$  / Normalization factor for cell  $j$

For each locBC, mean expression was calculated as the average normalized UMI count across all cells that expressed that locBC. Expression variance was calculated as the variance in normalized UMI counts across all cells that expressed that locBC.

#### ***Mean-independent noise (MIN) metric***

In order to remove the effect of the mean on the variance, we first fit a linear model:  $\log_2(\text{variance of IR location}) \sim \log_2(\text{mean of IR location})$  for each experimental pool and used the residuals of the model as the mean-independent noise metric. For each IR location, the MIN is the residual variance after removing the effect of the mean.

### **Analyses of genomic environment effects on mean-independent noise**

#### ***Chromatin environment association with mean/MIN***

We downloaded the Core 15-state chromHMM annotations for K562 cells from the Roadmap Epigenomics Project [21]. We then collapsed similar annotations and overlapped the IR locations with the corresponding annotation using the GenomicRanges R package [53].

We split the IRs into locations with high (top 50%) vs low (bottom 50%) mean/MIN, respectively. We then downloaded histone ChIP-seq datasets from ENCODE [35] (Additional file 9: Table S8) and plotted the signals 10 kb surrounding each class of IRs using the ComplexHeatmap package in R [54].

To look for enriched TF motifs, we first downloaded all human motifs from the HOCOMOCO v11 database. We then filtered the motifs for TFs that are expressed (FPKM  $\geq 1$ ) in the K562 cell line using whole-cell long poly(A) RNA-seq data generated by ENCODE (downloaded from the EMBL-EBI Expression Atlas, Additional file 9: Table S8). We then used the STREME package [36] (MEME suite 5.4.1) with sequences of 1 kb surrounding each IR to identify enriched de novo motifs in high or low MIN regions, using the other class as the control set of sequences (sequences enriched in high MIN vs low MIN and vice versa). We then took the top 2 motifs for each bin and matched it against a list of TFs expressed in K562s using TOMTOM [55] (MEME suite 5.4.1). We reported the top 6 TOMTOM matches.

### ***K562 Hi-C***

We performed Hi-C on wild-type K562 cells with the Arima Hi-C kit (A510008) according to the manufacturer's protocols (3 replicates, 870 million reads total). The reads were then processed with the Juicer pipeline [56] to generate HiC contact files for each replicate. We then used the peakHiC tool [57] to call loops from each IR with the following parameters: window size = 80, alphaFDR = 0.5, minimum distance = 10kb, qWr = 1. Using these parameters, each IR was looped to a median of 3 regions (range 0–7).

### ***Logistic regression model for intrinsic and extrinsic features associated with MIN***

We used chromatin modifications, TF motifs, GC content, whether or not the IR is in a gene, the number of enhancers looped to each IR, and number of ATAC-seq peaks surrounding each IR as features to train the model (full list of features in Additional file 3: Table S2). We used histone ChIP-seq and ATAC-seq datasets from ENCODE [35] (Additional file 9: Table S8) and overlapped their signals with each IR using bedtools v2.27.1 [58]. For all features, we considered the 20-kb upstream and downstream of each IR, respectively. For each histone modification, we computed the mean ChIP signal around the IRs. For ATAC-seq, we calculated the total number of peaks with the bedtools map count option. To look for TF motifs, we counted the numbers of each motif for TFs expressed in K562s (see above) in each surrounding IR sequence using FIMO [59] (MEME suite 5.0.4). Because this resulted in a long list of TFs, we further filtered the TFs to include only those with a significant correlation with MIN levels in the regression model. To determine the numbers of enhancers interacting with each IR, we annotated the loops called from peakHiC above with chromHMM enhancer annotations using the GenomicInteractions R package [60] and counted the number of enhancers.

For the extrinsic features, we calculated the proportion of cells in the “stem-like” substate and “differentiated” substate and different cell cycle phases based on the barcodes that appeared in those substates. We removed IR locations that have less than 30 cells in any of the substates.

We used the glm function in R (version 3.6.3) to fit logistic regression models. We separated the IR locations into top 20% MIN and bottom 20% MIN and used logistic regression to classify locations. We first fit a model with just local sequence features (chromatin modifications, number of TF motifs, number of loops, whether the IR location is in a gene, GC content, and the number of ATAC-seq peaks). We next fit a model with cellular information for each IR location: proportion of cells with data for the IR

location in S phase of the cell cycle, in G2 phase, and the proportion of cells that are in the “stem-like” substate of K562 cells [38]. Lastly, we fit a model that incorporated the extrinsic features and the significant predictors from the intrinsic features model. We used LOOCV to estimate model performance. We applied a similar approach to classify the top 20% mean locations from the bottom 20% mean locations.

### **Transcriptome analyses associated with SARGENT**

#### ***Processing the single-cell transcriptome data***

The single-cell RNAseq data was processed with CellRanger 6.0.1 and Scanpy 1.9.1 [61]. Briefly, the raw reads were processed with the standard single-cell expression cell line pipeline line. The resulting expression matrix was then imported into Scanpy for further visualization and clustering.

#### ***Identifying single-cell clones***

We identified the individual clones for Pool 4 which contained cells that grew out of 100 two-cell clones. Since most of the clones will have unique integrations into unique genomic locations, the cells that grew out from the same clone will have identical unique sets of locBCs. Due to the dropout rates associated with scRNAseq methods, not all barcodes will be present in all cells, nor will the cell barcodes be uniquely linked to correct sets of locBCs. To identify the barcodes belonging to the same clone, we first recorded locBCs that are linked by a given cell barcode. We then filtered the locBC list associated with a given cellBC based on the number of UMIs associated with these locBC. At this step, we used a knee point detection algorithm [62] that automatically detects the inflection point of the ordered UMI counts histogram. After filtering for locBCs that appear in more than five cells, we constructed a clonal graph by linking locBCs that co-occur in the same cells.

#### ***Validation of individual clones***

We extracted gDNA from 16 clones that were grown out from Pool 4. We then amplified the barcodes from each clone using Q5 High Fidelity 2× Master Mix (M0492, New England Biolabs) with primers specific to our reporter gene (CAS P58-59). For each clone, we performed four PCRs and pooled the PCRs for purification; 4 ng from each clone was then further amplified with 2 rounds of PCR to add Illumina sequencing adapters (CAS P60-63). The barcodes were sequenced on the Illumina NextSeq platform.

#### ***Estimating intrinsic vs extrinsic noise***

To understand how cellular environments affect IR expression, we first computed the mean and standard deviation from all IR locations in the same cell. Since standard deviation is expected to increase with mean, we calculated the coefficient of variation (CV, standard deviation of all IRs and divided it by the mean of all IRs for each cell) (Additional file 10: Table S9). To establish the null distributions, we randomly shuffled the cell labels for each clone and computed CVs for the shuffled cells.

Intrinsic and extrinsic noise were estimated using the statistical framework developed for the dual-reporter experiment [37]. In our experiment, single-cell expression differences among IR locations are treated as the intrinsic portion of the noise. We first

extracted the pairwise expression level for IR locations in every single cell. We then applied the statistical framework developed by Fu and Pachter [37]. The derivation is abbreviated and can be found in the original publication. Briefly, let  $C$  denote the expression for the first locBC in the cell,  $Y$  denote the expression for the second locBC in the cell, and  $n$  denote the number of cells.

Let  $\eta_{\text{ext}}$  denote the extrinsic noise, and it can be calculated as:

$$\eta_{\text{ext}} = \frac{1}{a\overline{C}\overline{Y}} \left( \sum_{i=1}^n C_i Y_i - n\overline{C}\overline{Y} \right)$$

where

$$a = (n - 1) \left( 1 + \frac{1}{n} \right) + \frac{1}{\rho^2}$$

$$\rho = \frac{\text{Cov}[C, Y]}{\sqrt{\text{Var}[C]} \sqrt{\text{Var}[Y]}}$$

Similarly, let  $\eta_{\text{int}}$  denote the intrinsic noise, and it can be calculated as:

$$\eta_{\text{int}} = \frac{1}{2a\overline{C}\overline{Y}} \left( \sum_{i=1}^n (C_i - Y_i)^2 - n(\overline{C} - \overline{Y})^2 \right)$$

where

$$a = \frac{2n^3 - 7n + 6}{2(n^2 - n)} + \frac{2 - n}{n^2 - n} \frac{\rho}{1 - \rho} + \frac{1}{2(n^2 - n)} \left( \frac{2}{1 - \rho} \right)^2$$

$$\rho = \frac{\text{Cov}[C, Y]}{\sqrt{\text{Var}[C]} \sqrt{\text{Var}[Y]}}$$

### ***Cell substate impact on expression mean and noise***

To compute cell substate specific expression mean and noise at different genomic locations, individual cells were assigned a cell cycle phase of G1, S, or G2/M using a previously reported set of cell-cycle-specific marker genes with Scanpy 1.9.1 [61]. For the stem-like substate analysis, we clustered cells based on their transcriptomes and assigned cells in the CD24 high cluster as CD24+ cells [38]. To ensure an accurate measurement of expression mean and noise, genomic locations with less than 15 cells in any phase were excluded from the cell cycle analysis. Based on this filtering criterion, 345 out of 939 genomic locations were used for this analysis. To determine the impact of cellular substates on gene expression noise, we calculated the proportion of cells in different cellular substates for each clone. For each clone, we also calculated the average mean and variance of all the IRs in that clone.

### ***Transgene integration analysis***

To examine whether the integration of a trans-gene alters endogenous gene expression, we first identified IR locations that were integrated into a gene body. Since the IR

insertion only occurs in a single clone, we computed pseudobulk expression from cells in the clone using decouplerR 1.1.0 [63]. We then randomly sampled the same number of cells from all the other clones and used the pseudobulk expression from these cells as wild-type expression. To determine whether the expression in the IR clone is significantly different from wild-type expression, we computed the *p*-value of differential expression using Fisher's exact test.

### Supplementary Information

The online version contains supplementary material available at <https://doi.org/10.1186/s13059-024-03277-9>.

Additional file 1: Supplementary Figures.  
Additional file 2: Table S1. List of all IR locations.  
Additional file 3: Table S2. Logistic regression results for MIN.  
Additional file 4: Table S3. Logistic regression results for mean.  
Additional file 5: Table S4. Mapping file of barcodes to clones.  
Additional file 6: Table S5. Effect of insertion on endogenous gene.  
Additional file 7: Table S6. Primers used in this study.  
Additional file 8: Table S7. Probes used for ClampFISH.  
Additional file 9: Table S8. List of datasets from ENCODE.  
Additional file 10: Table S9. Flux indices of clones.  
Additional file 11: Review history.

### Acknowledgements

We thank the members of the Cohen Lab for their helpful comments and critical feedback on the manuscript. We are also grateful to Jessica Hoisington-Lopez and MariaLynn Crosby in the DNA Sequencing Innovation Lab for assistance with high-throughput sequencing, the Genome Engineering and iPSC Center for kindly allowing us to use their flow cytometer for cell sorting, and the Hope Center DNA/RNA Purification Core at Washington University School of Medicine for helping with gDNA extractions.

### Peer review information

Wenjing She was the primary editor of this article and managed its editorial process and peer review in collaboration with the rest of the editorial team.

### Review history

The review history is available as Additional file 11.

### Authors' contributions

A.R, S.Z, C.K.Y.H, and B.A.C conceived and designed the project. S.Z, A.R, and C.K.Y.H designed and conducted all experiments and analyses. All authors wrote and edited the manuscript. C.K.Y.H, A.R, and S.Z contributed equally to this project.

### Funding

Institute: R01HG012304 (Dr. Barak Cohen) and National Institute of General Medical Sciences: R01GM092910 (Dr. Barak Cohen).

### Availability of data and materials

The raw single-cell and bulk RNA sequencing data from this publication are available from GEO under the accession number GSE223371 [64] and GSE266730 [65]. Analysis code used for the analysis of trio data are available with the MIT license on Github [66] and on Zenodo [67].

### Declarations

#### Ethics approval and consent to participate

Not applicable.

#### Consent for publication

Not applicable.

#### Competing interests

B.A.C is on the scientific advisory board of Patch Biosciences.

Received: 7 December 2022 Accepted: 13 May 2024

Published online: 24 May 2024

## References

1. Raj A, van Oudenaarden A. Nature, nurture, or chance: stochastic gene expression and its consequences. *Cell*. 2008;135:216–26.
2. Chang HH, Hemberg M, Barahona M, Ingber DE, Huang S. Transcriptome-wide noise controls lineage choice in mammalian progenitor cells. *Nature*. 2008;453:544–7.
3. Kalmar T, et al. Regulated fluctuations in nanog expression mediate cell fate decisions in embryonic stem cells. *PLoS Biol*. 2009;7:e1000149.
4. Abranches E, et al. Stochastic NANOG fluctuations allow mouse embryonic stem cells to explore pluripotency. *Development*. 2014;141:2770–9.
5. Desai RV, et al. A DNA repair pathway can regulate transcriptional noise to promote cell fate transitions. *Science*. 2021;373(6557):eabc6506.
6. Spencer SL, Gaudet S, Albeck JG, Burke JM, Sorger PK. Non-genetic origins of cell-to-cell variability in TRAIL-induced apoptosis. *Nature*. 2009;459:428–32.
7. Topolewski P, et al. Phenotypic variability, not noise, accounts for most of the cell-to-cell heterogeneity in IFN- $\gamma$  and oncostatin M signaling responses. *Sci Signal*. 2022;15:eabd9303.
8. Weinberger LS, Burnett JC, Toettcher JE, Arkin AP, Schaffer DV. Stochastic gene expression in a lentiviral positive-feedback loop: HIV-1 Tat fluctuations drive phenotypic diversity. *Cell*. 2005;122:169–82.
9. Shaffer SM, et al. Rare cell variability and drug-induced reprogramming as a mode of cancer drug resistance. *Nature*. 2017;546:431–5.
10. Emert BL, et al. Variability within rare cell states enables multiple paths toward drug resistance. *Nat Biotechnol*. 2021;39:865–76.
11. Yang C, Tian C, Hoffman TE, Jacobsen NK, Spencer SL. Melanoma subpopulations that rapidly escape MAPK pathway inhibition incur DNA damage and rely on stress signalling. *Nat Commun*. 2021;12:1747.
12. Wu S, et al. Independent regulation of gene expression level and noise by histone modifications. *PLoS Comput Biol*. 2017;13:e1005585.
13. Weinberger L, et al. Expression noise and acetylation profiles distinguish HDAC functions. *Mol Cell*. 2012;47:193–202.
14. Walters MC, et al. Enhancers increase the probability but not the level of gene expression. *Proc Natl Acad Sci*. 1995;92:7125–9.
15. Dar RD, et al. Transcriptional burst frequency and burst size are equally modulated across the human genome. *Proc Natl Acad Sci USA*. 2012;109:17454–9.
16. Larson DR, et al. Direct observation of frequency modulated transcription in single cells using light activation. *Elife*. 2013;2:e00750.
17. Senecal A, et al. Transcription factors modulate c-Fos transcriptional bursts. *Cell Rep*. 2014;8:75–83.
18. Faure AJ, Schmiedel JM, Lehner B. Systematic analysis of the determinants of gene expression noise in embryonic stem cells. *Cell Systems*. 2017;5:471–484.e4.
19. Karlič R, Chung H-R, Lasserre J, Vlahovicek K, Vingron M. Histone modification levels are predictive for gene expression. *Proc Natl Acad Sci USA*. 2010;107:2926–31.
20. Akhtar W, et al. Chromatin position effects assayed by thousands of reporters integrated in parallel. *Cell*. 2013;154:914–27.
21. Kundaje A, et al. Integrative analysis of 111 reference human epigenomes. *Nature*. 2015;518:317–30.
22. Dey SS, Foley JE, Limsirichai P, Schaffer DV, Arkin AP. Orthogonal control of expression mean and variance by epigenetic features at different genomic loci. *Mol Syst Biol*. 2015;11:806.
23. Zhang T, Foreman R, Wollman R. Identifying chromatin features that regulate gene expression distribution. *Sci Rep*. 2020;10:20566.
24. Eling N, Morgan MD, Marioni JC. Challenges in measuring and understanding biological noise. *Nat Rev Genet*. 2019;20:536–48.
25. Elowitz MB, Levine AJ, Siggia ED, Swain PS. Stochastic gene expression in a single cell. *Science*. 2002;297:1183–6.
26. Ozbudak EM, Thattai M, Kurtser I, Grossman AD, van Oudenaarden A. Regulation of noise in the expression of a single gene. *Nat Genet*. 2002;31:69–73.
27. das Neves RP, et al. Connecting variability in global transcription rate to mitochondrial variability. *PLoS Biol*. 2010;8:e1000560.
28. Stewart-Ornstein J, Weissman JS, El-Samad H. Cellular noise regulons underlie fluctuations in *Saccharomyces cerevisiae*. *Mol Cell*. 2012;45:483–93.
29. Sanchez A, Golding I. Genetic determinants and cellular constraints in noisy gene expression. *Science*. 2013;342:1188–93.
30. Raser JM, O’Shea EK. Noise in gene expression: origins, consequences, and control. *Science*. 2005;309:2010–3.
31. Zopf CJ, Quinn K, Zeidman J, Maheshri N. Cell-cycle dependence of transcription dominates noise in gene expression. *PLoS Comput Biol*. 2013;9:e1003161.
32. Hoffman MM, et al. Integrative annotation of chromatin elements from ENCODE data. *Nucleic Acids Res*. 2013;41:827–41.
33. Vallania FLM, et al. Origin and consequences of the relationship between protein mean and variance. *PLoS One*. 2014;9:e102202.
34. Bar-Even A, et al. Noise in protein expression scales with natural protein abundance. *Nat Genet*. 2006;38:636–43.
35. ENCODE Project Consortium. An integrated encyclopedia of DNA elements in the human genome. *Nature*. 2012;489:57–74.
36. Bailey TL. STREME: aAccurate and versatile sequence motif discovery. *Bioinformatics*. 2021. <https://doi.org/10.1093/bioinformatics/btab203>.
37. Fu AQ, Pachter L. Estimating intrinsic and extrinsic noise from single-cell gene expression measurements. *Stat Appl Genet Mol Biol*. 2016;15:447–71.
38. Litzenburger UM, et al. Single-cell epigenomic variability reveals functional cancer heterogeneity. *Genome Biol*. 2017;18:15.

39. Moudgil A, et al. Self-reporting transposons enable simultaneous readout of gene expression and transcription factor binding in single cells. *Cell*. 2020;182:992–1008.e21.
40. Wang, Q. et al. The mean and noise of stochastic gene transcription with cell division. *Math Biosci Eng*. 2018; 15: 1255–1270. Preprint at <https://doi.org/10.3934/mbe.2018058>.
41. Aznauryan, E. et al. Discovery and validation of human genomic safe harbor sites for gene and cell therapies. *Cell Rep Methods*. 2022; 2: 100154 Preprint at <https://doi.org/10.1016/j.crmeth.2021.100154>.
42. Papapetrou EP, Schambach A. Gene insertion into genomic safe harbors for human gene therapy. *Mol Ther*. 2016;24:678–84.
43. Bonny AR, Fonseca JP, Park JE, El-Samad H. Orthogonal control of mean and variability of endogenous genes in a human cell line. *Nat Commun*. 2021;12:292.
44. Raj A, Peskin CS, Tranchina D, Vargas DY, Tyagi S. Stochastic mRNA synthesis in mammalian cells. *PLoS Biol*. 2006;4:e309.
45. Benzinger D, Khammash M. Pulsatile inputs achieve tunable attenuation of gene expression variability and graded multi-gene regulation. *Nat Commun*. 2018;9:3521.
46. Michaels YS, et al. Precise tuning of gene expression levels in mammalian cells. *Nat Commun*. 2019;10:818.
47. Pavani G, Amendola M. Targeted gene delivery: where to land. *Front Genome Ed*. 2020;2:609650.
48. Cao J, et al. Comprehensive single-cell transcriptional profiling of a multicellular organism. *Science*. 2017;357:661–7.
49. Rosenberg AB, et al. Single-cell profiling of the developing mouse brain and spinal cord with split-pool barcoding. *Science*. 2018;360:176–82.
50. Qi Z, et al. An optimized, broadly applicable piggyBac transposon induction system. *Nucleic Acids Res*. 2017;45:e55.
51. Li H, Durbin R. Fast and accurate short read alignment with Burrows-Wheeler transform. *Bioinformatics*. 2009;25:1754–60.
52. Rouhanifard SH, et al. ClampFISH detects individual nucleic acid molecules using click chemistry-based amplification. *Nat Biotechnol*. 2018. <https://doi.org/10.1038/nbt.4286>.
53. Lawrence M, et al. Software for computing and annotating genomic ranges. *PLoS Comput Biol*. 2013;9:e1003118.
54. Gu Z, Eils R, Schlesner M, Ishaque N. EnrichedHeatmap: an R/Bioconductor package for comprehensive visualization of genomic signal associations. *BMC Genomics*. 2018;19:234.
55. Gupta S, Stamatoyannopoulos JA, Bailey TL, Noble WS. Quantifying similarity between motifs. *Genome Biol*. 2007;8:R24.
56. Durand NC, et al. Juicer provides a one-click system for analyzing loop-resolution Hi-C experiments. *cells*. 2016;3:95–8.
57. Bianchi, V. et al. Detailed regulatory interaction map of the human heart facilitates gene discovery for cardiovascular disease. *bioRxiv*. 2019; 705715. <https://doi.org/10.1101/705715>.
58. Quinlan AR, Hall IM. BEDTools: a flexible suite of utilities for comparing genomic features. *Bioinformatics*. 2010;26:841–2.
59. Grant CE, Bailey TL, Noble WS. FIMO: scanning for occurrences of a given motif. *Bioinformatics*. 2011;27:1017–8.
60. Harmston N, Ing-Simmons E, Perry M, Barešić A, Lenhard B. GenomicInteractions: an R/Bioconductor package for manipulating and investigating chromatin interaction data. *BMC Genomics*. 2015;16:963.
61. Wolf FA, Angerer P, Theis FJ. SCANPY: large-scale single-cell gene expression data analysis. *Genome Biol*. 2018;19:15.
62. Satopaa V, Albrecht J, Irwin D, Raghavan B. Finding a 'Kneedle' in a haystack: detecting knee points in system behavior. 2011 31st International Conference on Distributed Computing Systems Workshops. 2011: 166–171.
63. Badia-i-Mompel P, et al. decoupleR: ensemble of computational methods to infer biological activities from omics data. *Bioinformatics Adv*. 2022;2:vbac016.
64. Clarice KY Hong, Avinash Ramu, Siqi Zhao, Barak A Cohen. Effect of genomic and cellular environments on gene expression noise. Expression profiling data. 2023. <https://www.ncbi.nlm.nih.gov/geo/query/acc.cgi?acc=GSE223371>.
65. Clarice KY Hong, Avinash Ramu, Siqi Zhao, Barak A Cohen. Effect of genomic and cellular environments on gene expression noise. Expression profiling data. 2024. <https://www.ncbi.nlm.nih.gov/geo/query/acc.cgi?acc=GSE266730>.
66. Hong Clarice, Ramu Avinash, Zhao Siqi. castools: Command line tools and analysis code for the SARGENT project. GitHub. 2024. <https://github.com/barakcohenlab/castools>.
67. Clarice KY Hong, Avinash Ramu, Siqi Zhao, Barak A Cohen. Effect of genomic and cellular environments on gene expression noise (v1.0.2). Zenodo. 2024. <https://doi.org/10.5281/zenodo.10616403>.

## Publisher's Note

Springer Nature remains neutral with regard to jurisdictional claims in published maps and institutional affiliations.